Investigation of the elastic behavior of reciprocal systems using homogenization techniques

Lorenzo Greco, Arthur Lebée, Cyril Douthe

Investigation of the elastic behavior of reciprocal systems using homogenization techniques

Lorenzo Greco[1], Arthur Lebée[2], Cyril Douthe[3]

[1]MSc. Student, Universitá di Pisa, Italy, *lorenzo.greco@gmail.com*
[2]Researcher, Université Paris-Est, Laboratoire Navier (École des Ponts ParisTech, IFSTTAR, CNRS) Marne la Vallée, France, *arthur.lebee@enpc.fr*
[3]Researcher, Universié Paris-Est, IFSTTAR, France. *cyril.douthe@ifsttar.fr*

Summary: In this paper, the authors endeavour to develop design formulas for reciprocal systems using homogenization techniques. The theoretical background for homogenizing periodic beams systems as Kirchhoff-Love plates is first recalled. Then it is applied to a square reciprocal system. It is found that only biaxial bending (i.e. positive Gaussian curvature) generates stress inside the beams so that the equivalent plate model is a degenerated Kirchhoff-Love which is fully detailed. Then, some optimal configurations are investigated in terms of bending stiffness and strength. Finally, in order to validate the approach, full finite element simulations of simply supported reciprocal systems on square boundaries are compared with the homogenized solution previously derived. The convergence of the model and its accuracy for reasonable scale ratio is confirmed.

Keywords: *Nexorade, Kirchhoff-Love plate theory, Homogenization, Periodic plates, Space frame*

1. INTRODUCTION

"Reciprocal system" is an expression that designates a specific family of structures which has its roots in very old traditional construction systems in various regions of the world. Some examples can be found in traditional 12th century roofing structures in Japan as well as in manuscripts from the French architect Villard de Honnecourt or the Italian scholar Leonardo da Vinci [1]. This particular structural system can be seen as a construction technique to cover large spaces with short members assembled together with very simple connections [2]: traditionally, for stone architecture, connections are considered as compressed and unidirectional joints [3] but, in many recent applications, connections are made of spherical joints [4, 5]. The reciprocal character of the system comes from the fact that locally every member is supported by and supports its neighbours in a cyclic way as illustrated in Figure 1 (many other examples of reciprocal assemblies can be found in [2]). To describe this kind of assembly, Baverel *et al.* [6] suggested that a reciprocal system, also called a "nexorade", can be seen as a traditional structure in which members converging at a node would have been engaged within this node and thus proposed to call "engagement length" the length of the member which has entered the connection and "engagement window" the opening formed by the engagement of the members within the node. They then defined some other geometrical properties to characterise end dispositions but it is not necessary to recall them here as the only configuration that will be investigated in this paper is that of Figure 1.

Considering structural behaviour, researchs have been mainly dedicated to the investigation of some particular configurations or some particular structures [5, 7, 4, 3]. In these studies, the authors observed many interesting phenomena and relationships which are quite characteristic of the behaviour of reciprocal systems. For instance, about the way the transverse load is "circulating" from the interior of the surface to the supports, Gelez *et al* [8] pointed out that global bending of the "grid" generates additional local bending and large shear forces and that, more surprisingly for a simply supported structure, the shear forces in the members were maximum at mid-span whereas it is classically acknowledged that shear forces are maximum close to the supports. Likewise Douthe and Baverel [4] or Sanchez and Escrig [5] evidenced a strong link between the engagement length, inner bending moments and bending stiffness of the system. However, from a design point of view, there are actually no practical recommendations or formulas giving the influence of the various parameters on, for example, the global deflection of a reciprocal system or inner forces in the members. So, as the generation of complete reciprocal system (especially its geometry) is time consuming, the possibilities for optimisation and the variety of construction systems are practically reduced.

Though it is possible to give partial answers to these questions by means of homogenization techniques. The basic idea of homogenization consists in "seeing from far" the beams assembly which constitutes the nexorade. Indeed, even if the assembly is made of a well-defined periodic pattern at local scale, when zooming out, the pattern blurs until only a surface is seen.

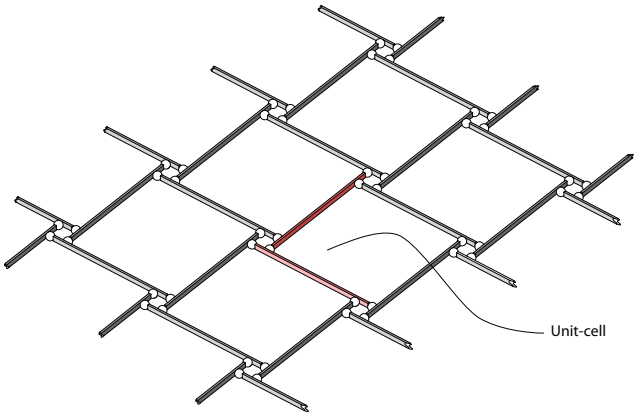

Fig. 1. Nexorade pattern

In mathematical terms, this procedure consists in separating scales: macroscopically the engineer wants to see an equivalent shell or plate model and microscopically he does not want to miss the detail of the stress state. Scale separation was rigorously established mathematically [9]. Based on this assumption in the linear elasticity framework, it is possible to derive a macroscopic model with an homogenized constitutive equation and also localization fields which enable the reconstruction of fields inside the unit-cell which generates the whole structure.

Here (Figure 1), the nexorade is made of few beams arranged in order to create a planar periodic pattern. The unit-cell which generates it, is constituted of only two beams (see red members in Figure 1). It will thus be possible to derive closed-form solutions of the localized resultants and moments which will be induced by the macroscopic plate fields. The corresponding plate model, that of the macroscopic surface, will be a Kirchhoff-Love plate model whose equivalent bending stiffness will be derived mathematically and investigated. Let us precise here that, if generally homogenization techniques are used to reduce the computational burden by separating scales, in the present case, it is obviously straightforward and accurate to compute directly the full structure, so that a gain is only expected in terms of parametric study: homogenisation techniques will avoid the necessity for generating numerous models with different geometries. And, apart from this aspect, our intention is to reveal some interesting features about the intrinsic behaviour of these periodic structures and to infer their consequences on preliminary design.

The paper is thus organized as follows. In section 2, the theoretical background for homogenizing nexorades as Kirchhoff-Love plates is recalled from [10]. Then it is applied to a square nexorade (section 3). It will be found that only biaxial bending (i.e. positive Gaussian curvature) gener-

ates stress inside the beams. This leads to a degenerated Kirchhoff-Love equivalent plate which is fully detailed. Then, because the unit-cell depends on very few parameters, some optimal configurations will be investigated in terms of bending stiffness or strength in section 4. Finally, in order to validate our approach, full finite element simulations of simply supported reciprocal systems on square boundaries will be compared with the homogenized solution previously derived (section 5).

2. HOMOGENIZATION OF A PERIODIC SPACE FRAME AS A KIRCHHOFF-LOVE PLATE

In this section we recall the main features of the Kirchhoff-Love plate theory and the corresponding homogenization scheme which was introduced in [10].

2.1. Brief summary of the Kirchhoff-Love plate model

We consider a linear elastic plate which mid-plane is the 2D domain $\omega \subset \mathbb{R}^2$. Cartesian coordinates (x_1, x_2, x_3) in the reference frame $(\hat{\underline{e}}_1, \hat{\underline{e}}_2, \hat{\underline{e}}_3)$ are used to describe macroscopic fields. At this stage, the microstructure of the plate is not specified. However, we assume that it is symmetric with respect to the mid-plane ω in order to uncouple the bending from the membrane stresses (this symmetry is often called mirror symmetry). Hence in the following, only the bending behavior of the equivalent plate will be derived.

The bending moment $M_{\alpha\beta}$ is the usual generalized stress for plates under bending[1]. Equilibrium equations and stress boundary conditions are gathered in the set of statically compatible fields:

$$\begin{cases} \underset{\sim}{\boldsymbol{M}} : \left(\underline{\nabla} \otimes \underline{\nabla}\right) + p_3 = 0 \text{ on } \omega & \text{(1a)} \\ (\underset{\sim}{\boldsymbol{M}} \cdot \underline{\boldsymbol{n}}) \cdot \underline{\boldsymbol{n}} = M^d \text{ on } \partial\omega^s & \text{(1b)} \\ (\underset{\sim}{\boldsymbol{M}} \cdot \underline{\nabla}) \cdot \underline{\boldsymbol{n}} + \dfrac{\partial (\underset{\sim}{\boldsymbol{M}} \cdot \underline{\boldsymbol{n}}) \cdot \underline{\boldsymbol{t}}}{\partial s} = q_3^d \text{ on } \partial\omega^s & \text{(1c)} \end{cases}$$

where $\partial\omega^s$ is the portion of edge on which static boundary conditions apply and $\underline{\boldsymbol{n}}, \underline{\boldsymbol{t}}$ the related outer normal and tangent vectors; s the corresponding curvilinear coordinate. M^d is the tangential bending moment per unit length and q_3^d the out-of-plane force per unit length enforced on the edge. The plate is loaded with the distributed force $\hat{\underline{\boldsymbol{p}}} = p_3 \hat{\underline{\boldsymbol{e}}}_3$.

The bending moment $\underset{\sim}{\boldsymbol{M}}$ works with $\underset{\sim}{\boldsymbol{K}}$ the curvature:

$$K_{\alpha\beta} = -U_{3,\alpha\beta} \tag{2}$$

where U_3 is the average of the plate out-of-plane displacement. The corresponding boundary conditions are:

$$\begin{cases} -\left(U_3 \underline{\nabla}\right) \cdot \underline{\boldsymbol{n}} = \theta^d \text{ on } \partial\omega^k & \text{(3a)} \\ U_3 = U_3^d \text{ on } \partial\omega^k & \text{(3b)} \end{cases}$$

where $\partial\omega^k$ is the portion of edge on which kinematic boundary conditions apply: U_3^d is a given displacement and θ^d is the rotation with respect to the tangent vector on the edge.

Finally, the Kirchhoff-Love plate constitutive equation writes as:

$$\underset{\sim}{\boldsymbol{M}} = \underset{\approx}{\boldsymbol{D}} : \underset{\sim}{\boldsymbol{K}} \tag{4}$$

where $\underset{\approx}{\boldsymbol{D}}$ is the the flexural stiffness. It is a planar fourth-order tensor. The constitutive tensor $\underset{\approx}{\boldsymbol{D}}$ is function of the plate microstructure. Its derivation is based on the homogenization scheme discussed in the next section.

[1] Vectors and higher-order tensors are boldfaced and different underlinings are used for each order: vectors are straight underlined, $\underline{\boldsymbol{u}}$. Second order tensors are underlined with a tilde: $\underset{\sim}{\boldsymbol{M}}$. Fourth order tensors are are doubly underlined with a tilde: $\underset{\approx}{\boldsymbol{D}}$.

When dealing with plates, both 2-dimensional (2D) and 3D tensors are used. Thus, $\hat{\underline{\boldsymbol{T}}}$ denotes a 3D vector and $\underline{\boldsymbol{T}}$ denotes a 2D vector or the in-plane part of $\hat{\underline{\boldsymbol{T}}}$. The same notation is used for higher-order tensors: $\hat{\underset{\sim}{\sigma}}$ is the 3D second-order stress tensor while $\underset{\sim}{\sigma}$ is its in-plane part. When dealing with tensor components, the indexes specify the dimension: a_{ij} denotes the 3D tensor $\hat{\underset{\sim}{\boldsymbol{a}}}$ with Latin index $i, j, k.. = 1, 2, 3$ and $a_{\alpha\beta}$ denotes the 2D tensor $\underset{\sim}{\boldsymbol{a}}$ with Greek indexes $\alpha, \beta, \gamma.. = 1, 2$.

2.2. Homogenization scheme

When the plate is laminated, closed-form expression for $\underset{\approx}{\boldsymbol{D}}$ can be derived (see [11] for instance). When the plate is periodic this tensor must be derived using an homogenization procedure. This procedure relies on the fundamental assumption that loadings as well as macroscopic variables ($\underset{\sim}{\boldsymbol{M}}$ and $\underset{\sim}{\boldsymbol{K}}$) varies slowly compared to the size of the microstructure (the unit-cell). Then, it is possible to define auxiliary problems which enable the derivation of the actual microscopic fields as a linear superposition of macroscopic fields. Once this is done, we take the average of the elastic energy stored inside the unit-cell and equate it to the macroscopic elastic energy density (namely the macroscopic constitutive equation). This analogy between micro and macroscopic energy is usually called Hill-Mandel principle. When the plate microstructure is constituted of a 3D continuum, the auxiliary problems were introduced in [12]. In the present case, we consider periodic plates whose unit-cell is constituted of connected beams: a "space frame". This necessitates the adaptation of the homogenization scheme for 3D continuum which was suggested in [10]. In this section, we first describe the unit-cell and the related beam model, the Kirchhoff-Love auxiliary problem which enables the derivation of $\underset{\approx}{\boldsymbol{D}}$ for this type of plate.

2.2.1. The unit-cell of the space frame

In this section, we give a general description of the space frame and set the main assumptions. We also introduce some useful definitions.

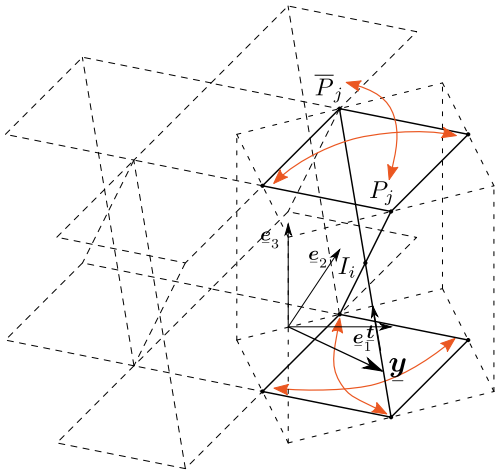

Fig. 2. unit-cell of a space frame with four pairs of periodicity nodes and one interior node.

We consider an in-plane periodic plate which unit-cell is made of an assembly of connected beams (Figure 2). The unit-cell reference frame is $(\hat{\underline{e}}_1, \hat{\underline{e}}_2, \hat{\underline{e}}_3)$ associated with the local coordinate $\underline{y} = (y_1, y_2, y_3)$. It is symmetric with respect to its mid-plane.

There are n_b beams constituting the unit-cell intersecting at nodes (see Figure 2). Each beam connects two nodes through a path γ_k. The collection of γ_k is $\Gamma = \cup_{k=1}^{n_b} \gamma_k$. Without loss of generality, we assume in this section a perfect connection at nodes (fully clamped). Furthermore, a subset of these nodes are pairs of periodicity nodes: they connect the unit-cell to its neighbors. Thus interior nodes are denoted I_i $(i = 1, n_i)$ and periodicity pairs P_j and $\overline{P}_j$, $(j = 1, n_p)$.

Local beam equations The local reference frame along each beam is denoted $(\hat{\underline{t}}, \hat{\underline{n}}, \hat{\underline{b}})$ associated with the coordinate $\underline{s} = (s_1, s_2, s_3)$. The unit vector $\underline{t}$ is oriented in the direction of the neutral axis of the beam. For the sake of simplicity, beams are assumed rectilinear and follows St Venant's approximation with uniform torsion. Consequently, the resultant force $\underline{r}$ and the moments $\underline{m}$ are defined as follows:

$$\hat{\underline{r}} = \int_S \hat{\underset{\sim}{\sigma}}^B \cdot \hat{\underline{t}} \, dS \quad \text{and} \quad \hat{\underline{m}} = \int_S \hat{\underline{s}} \times \left(\hat{\underset{\sim}{\sigma}}^B \cdot \hat{\underline{t}}\right) dS \tag{5}$$

where $\mathcal{S}$ is the beam section, $\hat{\underset{\sim}{\sigma}}^B$ is the beam's local 3D stress and $\times$ denotes the cross product.

Each beam is free of distributed load. The corresponding local equilibrium equations are:

$$\begin{cases} \hat{\underline{r}}' = 0 \\ \hat{\underline{m}}' + \hat{\underline{t}} \times \hat{\underline{r}} = 0 \end{cases} \tag{6}$$

Where " $'$ " denotes the derivative with respect to s_1. The constitutive equation writes as follows:

$$\begin{cases} \hat{\underline{r}} = \hat{\underset{\sim}{E}} \cdot \left(\hat{\underline{u}}' + \hat{\underline{t}} \times \hat{\underline{\theta}} \right) \\ \hat{\underline{m}} = \hat{\underset{\sim}{G}} \cdot \hat{\underline{\theta}}' \end{cases} \tag{7}$$

where $\hat{\boldsymbol{u}}$ is the beam displacement and $\hat{\boldsymbol{\theta}}$ its rotation. $\hat{\underset{\sim}{E}}$ and $\hat{\underset{\sim}{G}}$ are the beam stiffness tensors. For instance, when there are two axis of symmetry for the section, these tensors write in the local reference frame of the beam $(\hat{\underline{t}}, \hat{\underline{n}}, \hat{\underline{b}})$, as:

$$\hat{\underset{\sim}{E}} = \begin{pmatrix} E\mathcal{S} & 0 & 0 \\ 0 & G\mathcal{S}_{s,2} & 0 \\ 0 & 0 & G\mathcal{S}_{s,3} \end{pmatrix} \text{ and } \hat{\underset{\sim}{G}} = \begin{pmatrix} G\mathcal{J} & 0 & 0 \\ 0 & E\mathcal{I}_2 & 0 \\ 0 & 0 & E\mathcal{I}_3 \end{pmatrix} \tag{8}$$

where E is the Young modulus, G the shear modulus of the constitutive material of the beam. $\mathcal{S}$ is the section area, $\mathcal{S}_{s,2}$ and $\mathcal{S}_{s,3}$ are the shear areas in each direction. $\mathcal{J}$ is the torsion constant, $\mathcal{I}_2 = \int_{\mathcal{S}} s_3^2 d\mathcal{S}$ and $\mathcal{I}_3 = \int_{\mathcal{S}} s_2^2 d\mathcal{S}$ are the second moments of inertia.

Kinematic and static constraints on the assembly Since we assumed perfect connection, displacements and rotations must be continuous at interior nodes I_i in all the following.

Moreover, local equilibrium at each interior node must be fulfilled:

$$\forall j = 1...n_i, \quad \sum_{k=1}^{n_{bj}} \epsilon_k \, {}^k\hat{\underline{r}}\left(I_j\right) = 0 \quad \text{and} \quad \sum_{k=1}^{n_{bj}} \epsilon_k \, {}^k\hat{\underline{m}}\left(I_j\right) = 0 \tag{9}$$

where n_{bj} is the number of beams connecting at node I_j, ${}^k\hat{\underline{r}}$ denotes the resultant of beam k connected to the node. Moreover, $\epsilon_k = +1$ if ${}^k\underline{t}$, the tangent vector of beam k, is directed toward the node and $\epsilon_k = -1$ if ${}^k\underline{t}$ is directed away the node.

Additionally we define periodicity conditions as:

$$\forall j = 1...n_p, \quad \hat{\underline{\theta}}\left(P_j\right) = \hat{\underline{\theta}}\left(\overline{P}_j\right) \quad \text{and} \quad \hat{\underline{u}}\left(P_j\right) = \hat{\underline{u}}\left(\overline{P}_j\right) \tag{10}$$

Elastic energy The complementary elastic energy per unit surface stored inside the unit-cell will be used in the homogenization scheme. It is defined as the sum along Γ of the beams stress energy density:

$$w^{*\text{int}}\left(\hat{\underline{r}}, \hat{\underline{m}}\right) = \frac{1}{2A} \int_\Gamma \left({}^T\hat{\underline{r}} \cdot \hat{\underset{\sim}{E}}^{-1} \cdot \hat{\underline{r}} + {}^T\hat{\underline{m}} \cdot \hat{\underset{\sim}{G}}^{-1} \cdot \hat{\underline{m}} \right) d\Gamma \tag{11}$$

where A is the in-plane area of the unit-cell

2.2.2. Homogenization as Kirchhoff-Love plate

In this section, we recall the Kirchhoff-Love auxiliary problem in a suitable form for the unit-cell we just introduced:

$$\mathcal{P}^{(K)} : \begin{cases} \left(\hat{\underline{r}}^{(K)}\right)' = 0 \text{ on } \Gamma \\ \left(\hat{\underline{m}}^{(K)}\right)' + \hat{\underline{t}} \times \hat{\underline{r}}^{(K)} = 0 \text{ on } \Gamma \\ \hat{\underline{r}}^{(K)} = \hat{\underset{\sim}{E}} \cdot \left(\left(\hat{\underline{u}}^{(K)}\right)' + \hat{\underline{t}} \times \hat{\underline{\theta}}^{(K)} \right) \text{ on } \Gamma \\ \hat{\underline{m}}^{(K)} = \hat{\underset{\sim}{G}} \cdot \left(\hat{\underline{\theta}}^{(K)}\right)' \text{ on } \Gamma \\ \hat{\underline{u}}^{(K)} = \hat{\underline{u}}^{\text{per}} + \hat{\underline{U}}^{(K)} \text{ on } \Gamma \\ \hat{\underline{\theta}}^{(K)} = \hat{\underline{\theta}}^{\text{per}} + \hat{\underline{\Theta}}^{(K)} \text{ on } \Gamma \\ \forall i = 1...n_i, \quad \hat{\underline{u}}^{\text{per}} \text{ and } \hat{\underline{\theta}}^{\text{per}} \text{ continuous at node } I_i \\ \forall i = 1...n_i, \quad \hat{\underline{r}}^{(K)} \text{ and } \hat{\underline{m}}^{(K)} \text{ equilibrated at node } I_i \\ \forall j = 1...n_p, \quad \hat{\underline{u}}^{\text{per}}, \hat{\underline{\theta}}^{\text{per}}, \hat{\underline{r}}^{(K)} \text{ and } \hat{\underline{m}}^{(K)} \text{ periodic at node } P_j \end{cases} \tag{12}$$

Basically, this auxiliary problem consist in applying on average on the unit-cell the Kirchhoff-Love displacement field

$$\hat{\underline{U}}^{(K)} = y_3 \hat{\underset{\sim}{K}} \cdot \hat{\underline{y}} - \frac{1}{2} \left({}^T\hat{\underline{y}} \cdot \hat{\underset{\sim}{K}} \cdot \hat{\underline{y}} \right) \hat{\underline{e}}_3 \tag{13}$$

and the rotation field:

$$\hat{\underline{\Theta}}^{(K)} = \underset{\sim}{\omega} \cdot \hat{\underset{\sim}{K}} \cdot \hat{\underline{y}} \tag{14}$$

where $\underset{\sim}{\omega} = \left(\hat{\underline{e}}_2 \otimes \hat{\underline{e}}_1 - \hat{\underline{e}}_1 \otimes \hat{\underline{e}}_2 \right)$ is the permutation operator. We also introduced the convenient notation:

$$\hat{\underset{\sim}{K}} = \begin{pmatrix} K_{11} & K_{12} & 0 \\ K_{12} & K_{22} & 0 \\ 0 & 0 & 0 \end{pmatrix} \tag{15}$$

Finally the superscript "per" refers to periodicity: $\hat{\underline{u}}^{\text{per}}$ and $\hat{\underline{\theta}}^{\text{per}}$ are corrector fields which relaxes the actual deformation of the unit-cell compared to the exact Kirchhoff-Love kinematics $\hat{\underline{U}}^{(K)}, \hat{\underline{\Theta}}^{(K)}$.

Solving the problem for each individual component of $\underset{\sim}{K}$ leads to the stress localization tensors $r^K_{i\alpha\beta}$ and $m^K_{i\alpha\beta}$. The complete local stress field can be reconstructed by linear combination:

$$\hat{\underline{r}}^{(K)} = \left(r^K_{i\alpha\beta} K_{\alpha\beta} \right) = \hat{\underset{\sim}{r}}^K : \underset{\sim}{K} \tag{16a}$$

$$\hat{\underline{m}}^{(K)} = \left(m^K_{i\alpha\beta} K_{\alpha\beta} \right) = \hat{\underset{\sim}{m}}^K : \underset{\sim}{K} \tag{16b}$$

The flexural stiffness tensor is derived using Hill-Mandel principle. The Kirchhoff-Love plate energy density is identified to the energy stored in the unit-cell (Equation 11):

$$w^{\text{int}}\left(\hat{\underline{r}}^{(K)}, \hat{\underline{m}}^{(K)}\right) = \frac{1}{2} \underset{\sim}{K} : \underset{\sim}{D} : \underset{\sim}{K} \tag{17}$$

The flexural stiffness moduli are then evaluated as follows:

$$\underset{\sim}{D} = \frac{1}{A} \int_\Gamma \left({}^T\hat{\underset{\sim}{r}}^K \cdot \hat{\underset{\sim}{E}}^{-1} \cdot \hat{\underset{\sim}{r}}^K + {}^T\hat{\underset{\sim}{m}}^K \cdot \hat{\underset{\sim}{G}}^{-1} \cdot \hat{\underset{\sim}{m}}^K \right) d\Gamma \tag{18}$$

3. APPLICATION TO A SQUARE NEXORADE

There is a wide variety of nexorade assemblies [2], most of which leads to non-planar configurations because of eccentricities between members axes at connections. In the present paper, we consider only planar systems in order to fulfil periodicity requirement of homogenization techniques. This means that there are no eccentricity and that connections are designed so that members lay on the same plane. Still there are many different ways to realise plane tessellation with regular and semi-regular patterns [13]. Regular patterns consist of triangles, squares and hexagons; semi-regular of combinations of previous forms. For simplicity reasons and also practical engineering aspects [8], we focus here on square reciprocal systems (see Figure 1 and Figure 3). The unit-cell is thus constituted of only two beams. This enables the easy derivation of closed-form solutions for the auxiliary problem presented in the previous section. Actually, similar calculations have been conducted by the authors for the triangular and hexagonal unit-cells and the results are qualitatively the same as those which will be derived here.

3.1. The unit-cell

Figure 3 shows the unit-cell of the reciprocal system idealization. It is constituted of two beams which lay in the $(\hat{\underline{e}}_1, \hat{\underline{e}}_2)$ plane. Both beams are identical with a total length l. We assume that the beam section has two orthogonal axes of symmetry. One axis is $\hat{\underline{e}}_3$ so that the beam stiffness tensors write as Equation 8 in the local reference frame.

Every member is divided into three parts of length a or $b = l - 2a$ where a is called the engagement length [6, 2, 4]. The locations of the separation between the three parts correspond to connections between members: between two parts, another member extremity is supported on one side or

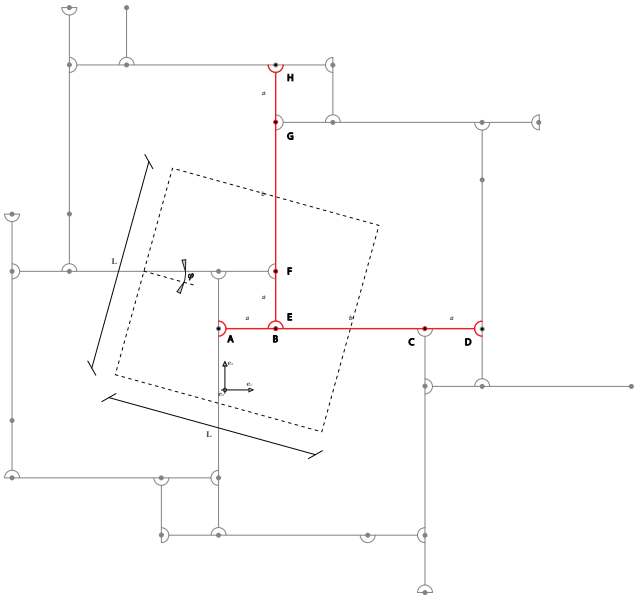

Fig. 3. The unit-cell of the square nexorade and its parameters.

the other. The connection is modelled as a perfect spherical joint whose center is located on the neutral axis of the supporting beam (this insures flatness of the unit-cell). Actually, this is an idealisation: in practical applications [8], the connection is always slightly eccentric which would add a slight amount of torsion in the members but would not affect the main conclusions of the present work.

Let us also point out that this choice makes the nexorade isostatic for the out-of-plane behavior [14], thus meaning that no prestress can be applied and that there is no redundancy in the system. In addition, this means that defects, members inertia and thermal loads do not influence inner stresses which can be evaluated only by static considerations. Besides, it was found in [8] that with this configuration the stress distribution is less affected by irregular boundaries than with more conventional structures such as beam lattices or slabs.

The choice of a and l fully sets the in-plane geometry of the system. However, in the following (see Figure 3), we will use another set of parameters which is more convenient for calculations and which are in accordance of the periodicity pattern of the system: the in-plane size of the unit-cell L and the rotation angle $\varphi \in]0, \frac{\pi}{4}]$ referring to the rotational way to generate a reciprocal system introduced in [15]. We have thus the corresponding relations between (a, l) and (L, φ):

$$a = L \sin\varphi \quad \text{and} \quad l = L(\cos\varphi + \sin\varphi) \tag{19}$$

The choice of L sets the scale separation between the unit-cell and the overall size of the nexorade. Varying φ enables to explore all possible engagement length a. The two limit cases are illustrated in Figure 4.The case $\varphi = 0$ corresponds to zero engagement length ($a = 0$) and cannot be reached in practice. The case $\varphi = \frac{\pi}{4}$ corresponds to $b = 0$ or $l = 2a$ which is the configuration that was actually used for the archaeological excavation shelter of Bibracte in France [7].

This reciprocal system is planar and symmetric with respect to its mid-plane. It thus uncouples membrane and flexural effects. The model proposed here concerns a system which is loaded perpendicularly to its plane, the present study will thus be limited to a first order plate theory where only flexural effects will be considered. Actually, the authors are working on the identification of the membrane properties to investigate the influence of membrane effects on the out-of-plane (more detailed will be shown in a coming paper). Moreover, it can be remarked that in addition to the periodicity of the pattern, the only invariance of the unit-cell is the $\frac{\pi}{2}$ rotation

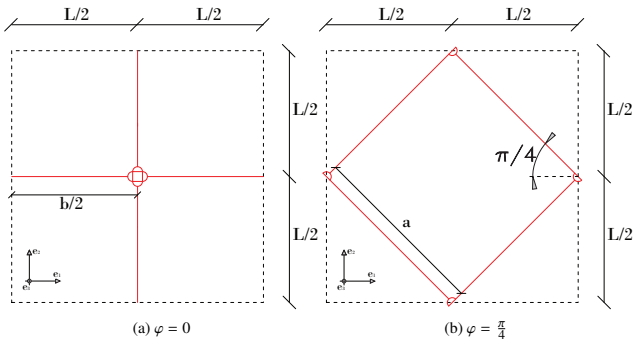

Fig. 4. The Nexorade unit-cell, for limit values of the angle φ

with respect to the out-of-plane axis, this pattern is hence chiral and one could expect surprising couplings (see [16] for instance) which are surely worth investigation.

3.2. Solution of the auxiliary problem

Solving the auxiliary problem (12) for the square nexorade does not present major difficulties and is not detailed here. We summarize here the main conclusions.

The auxiliary problem applies three out-of-plane curvatures on average on the unit-cell (pure bending in two directions and torsion). It turns out that only one equilibrated distribution of stress inside the beams is achievable. Hence the following static relations for the equivalent plate bending moment come out:

$$M_{12} = 0 \quad \text{and} \quad M_{11} = M_{22} \tag{20}$$

The mechanical meaning of these relations will be detailed in the next section. Let us first define the biaxial bending moment:

$$M \equiv M_{11} = M_{22} \tag{21}$$

Then, the only achievable local stress distribution which is related to the biaxial bending moment M is the out-of-plane four-point-bending of each beam as illustrated in Figure 5. The out-of-plane shear force in the beams is constant and maximum in the engagement windows, its amplitude is given by:

$$r^{(M)} = \frac{M}{\cos\varphi \sin\varphi} \tag{22}$$

The bending moment in the beams is linear in the engagement windows (see Figure 6) and reaches its maximum value in their central part which is:

$$m^{(M)} = \frac{ML}{\cos\varphi} \tag{23}$$

As expected from the general isostaticity of the system, it is remarked that these fields do not depend on the section characteristics of the members.

3.3. Degenerated Kirchhoff-Love model

The static relations which came out from the derivation of the auxiliary is typical from a degenerated plate model: some flexural stiffness moduli vanish and the constitutive tensor becomes non-elliptic. More precisely, for a general elliptic constitutive equation the rank of the bending stiffness tensor $\underset{\approx}{\boldsymbol{D}}$ is 3. In the present case, there are two static links (Equation 20) which make the bending stiffness degenerate to rank 1.

The first relation: $M_{12} = 0$ means that no macroscopic torsion bending is achievable inside the nexorade and that the equivalent plate is free to deform locally as a hyperbolic paraboloid. This free motion exists also in other structures such as cable nets, gridshells and was often used in order generate hypar shaped roofings.

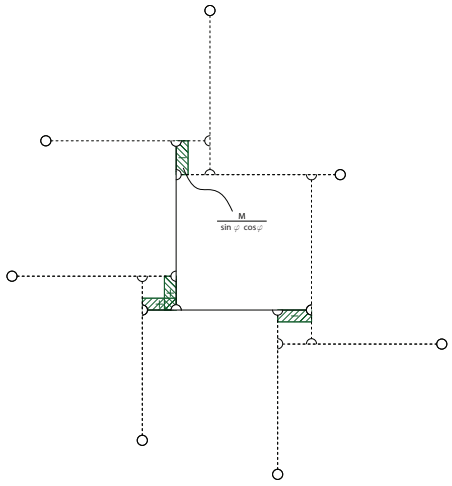

Fig. 5. Local out-of plane shear force in the beams induced by the biaxial macroscopic bending moment M.

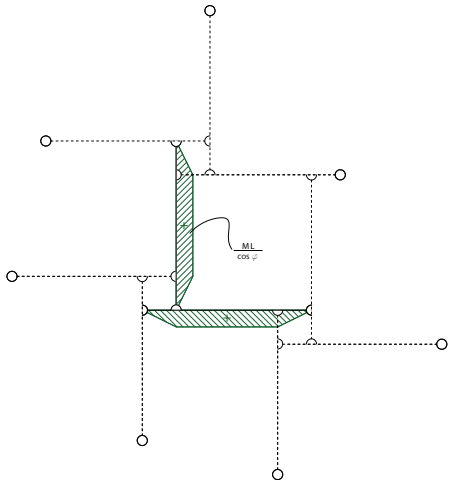

Fig. 6. Local bending moment in the beams induced by the biaxial macroscopic bending moment M.

The second relation: $M_{11} = M_{22}$ is less common and means that only strictly bi-axial bending is generating elastic energy. It is possible to show that the related free strain corresponds to strictly opposite main curvatures: $K_{11} = -K_{22}$.

There remains thus only one scalar stress field for the plate: the bi-axial bending moment M. This directly means that the degenerated plate model is isotropic (both static links which came out here can be retrieved, considering the bending stiffness of a homogeneous and isotropic plate for which the Poisson's ratio is set to $\nu = -1$). This isotropy means that, despite the rather low level of symmetry of the unit-cell, the orientation of the microstructure relatively to the global surface is indifferent, that the members directions relatively to those of the global plate has no influence on the stiffness of the structure. The flexural behaviour of the studied reciprocal system is thus completely defined by two lengths: l the length of the members and a their engagement length.

Now, considering the static relations (20) and the definition of the bi-axial bending moment M, it is possible to derive a simpler plate model for the nexorade than Kirchhoff-Love model. Indeed inserting (20) and M in the Kirchhoff-Love equilibrium equations (1) leads to the following statically admissible fields:

$$\begin{cases} \Delta M + p_3 = 0 \text{ on } \omega & \text{(24a)} \\ M = M^d \text{ on } \partial\omega^s & \text{(24b)} \\ (M \otimes \underline{\nabla}) \cdot \underline{\boldsymbol{n}} = q_3^d \text{ on } \partial\omega^s & \text{(24c)} \end{cases}$$

where the distinction between "simple soft support" or "hard simple support" vanish since the torsion bending moment is zero.

Taking the weak form of the equilibrium equation, it is then easy to demonstrate that the dual variable of the bi-axial bending moment M is twice the mean curvature:

$$K = \Delta U_3 \tag{25}$$

and that the kinematic boundary conditions remain the same as the full Kirchhoff-Love model:

$$\begin{cases} -\left(U_3 \underline{\nabla}\right) \cdot \underline{\boldsymbol{n}} = \theta^d \text{ on } \partial\omega^k & \text{(26a)} \\ U_3 = U_3^d \text{ on } \partial\omega^k & \text{(26b)} \end{cases}$$

The last missing part of the model is the constitutive equation which writes simply as:

$$K = dM \tag{27}$$

where d is the bi-axial bending compliance. This compliance is derived computing the elastic energy stored in the unit-cell per unit surface as function of M:

$$d = \frac{2L}{EI_2 \cos\varphi} \left(\frac{24EI_2}{GS_{s,3}L^2 \sin 2\varphi} + \left(1 - \frac{\tan\varphi}{3}\right) \right) \tag{28}$$

Introducing the characteristic lengths of the system (19) in (28) and inverting it, the stiffness of the system D turns out to:

$$D = \frac{EI_2}{2a} \left(\frac{(l-a)^2}{(l-a)^2 + a^2} \right) \left(\frac{3a\eta}{36a + (3l - 4a)\eta} \right) \tag{29}$$

where η is a parameter that represents the relative influence of shear stiffness in the members which is given by:

$$\eta = \frac{GS_{s,3}a^2}{EI_2} \tag{30}$$

One remarks that the reference length in η is a the engagement length which corresponds to the local lever arm of shear forces in the members. Hence, the smaller the engagement length, the larger the effect of shear deformation and the softer the structure. In the same way, for members with infinite shear rigidity or Euler-Bernouilli members, the stiffness of the reciprocal system becomes:

$$D_{Euler} = \frac{3EI_2}{2(3l - 4a)} \left(\frac{(l-a)^2}{(l-a)^2 + a^2} \right) \tag{31}$$

4. PARAMETRIC INVESTIGATION

In this section, a short discussion of preceding results is proposed to better understand the influence of the various design parameters on the behaviour of square reciprocal systems.

4.1. Stress inside the unit-cell

Figure 7 shows first the trends of the shear stress and bending moment as functions of the relative engagement length (a/l) which varies from 0 to 0.5. Both variables have been represented in a non dimensional form to keep the generality of the argument by introducing 19 in (22) and (23) respectively:

$$\frac{r^{(M)}}{M} = \frac{a^2 + (l-a)^2}{a(l-a)} \quad \text{and} \quad \frac{m^{(M)}}{M} = \frac{a^2 + (l-a)^2}{(l-a)} \tag{32}$$

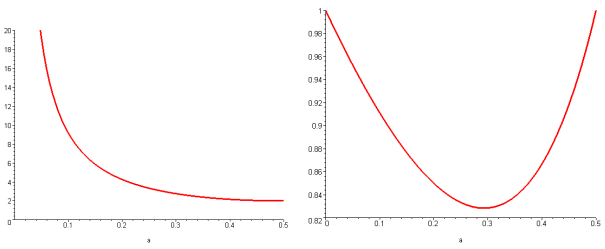

(a) Shear $\frac{r(M)}{M}$ as function of a/l (b) Moment $\frac{m(M)}{M}$ as function of a/l

Fig. 7. Shear and Moment in the Nexor, due to the plate bending moment

It is remarked in (32) that shear forces only depends on the relative engagement length a/l but not on the length l of the members, on the contrary to the bending moment which depends linearly on l. Decreasing the size of the members will thus decrease bending stresses but will have no influence on the shear stresses which will remain constant.

Concerning Figure 7a, it is first remarked that when a/l tends to 0, shear stress goes to infinite, no matter what are the plate moment or the other geometric parameters. Consequently, the equivalent stiffness (29 drops to 0 when the engagement length tends to 0, independently of the members rigidity. Taking into account shear rigidity in a reciprocal system model seems thus necessary, especially if small engagement length have to be investigated. However, it should be stressed that results for $a/l \to 0$ are of few practical interest, since for small engagement length, the joints would be hard to realise. Finally it is noticed that, since the shear stress is linearly dependent on the plate moment, the maximum shear will be found where the equivalent plate has the maximum bending moment as observed in [3, 8].

Concerning then Figure 7b, it is observed that the bending moment is bounded, contrary to shear forces. It is maximum for $a/l = 0$ and $a/l = 1/2$ and minimum for $a/l = (1 - \sqrt{2}/2) \approx 0.414$. This last value of the relative engagement length defines thus a configuration which minimises bending stresses in the members. The extrem values are given by:

$$m^M_{max} = Ml \quad \text{and} \quad m^M_{min} = Ml(2\sqrt{2} - 2) \approx 0.828 m^M_{max} \tag{33}$$

Finally, like for shear forces, as the moment is linearly dependent on the plate moment, the maximum moment will be found where the equivalent plate has the maximum moment. This result is in accordance with the ones found in practical cases [3, 8].

4.2. Bending stiffness

In order to investigate the influence of the members characteristics (section, length and engagement length) on the equivalent bending stiffness, the variations of D given by (29) have been plotted in Figure 8 as a function of the relative engagement length a/l. Four values of η/a^2 (10, 100, 1000 and 10000) have been chosen, corresponding to members with low shear rigidity to high shear rigidity. As expected, the higher the relative shear stiffness η/a^2, the higher the global plate stiffness. It is also remarkable that every curve presents a maximum value: this means that for a given section or a given relative shear stiffness, there is one engagement length which maximises the bending stiffness. For low values of η, the optimal relative engagement length a/l tends toward 0.3966 where as for high values of η it tends to 0.5. The intuition of the engineers of Bibracte's roofing in [7] is hence confirmed: would the members in [7] have been infinitely rigid in shear, they would have chosen the optimal configuration with $a = l/2$.

For reciprocal systems like for many other usual structural systems, there are thus two competing design strategies, one is to minimise stresses and the other is to minimise displacements. To give an idea for infinitely shear stiffness, choosing to privilege stresses and thus a configuration with $a/l = (1 - \sqrt{2}/2)$ leads to an increase of approximately 7% of the deflection,

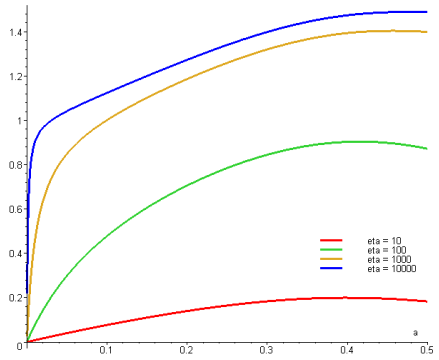

Fig. 8. Nexorade stiffness as function of a/l, for $\eta/a^2 = [10, 10000]$

whereas choosing to privilege stiffness and thus a configuration with $a/l = 1/2$ leads to an increase of approximately 20% of the bending stresses.

5. VALIDATION THROUGH FINITE ELEMENT SIMULATION

In the following, the analytical solution of a simply supported plate under distributed loading with the stiffness and localisation tensor identified in previous section is compared to a finite element simulation conducted with Abaqus.

5.1. Navier solution for the homogenized plate

The reference solution of the simply supported plate under distributed load is the one established by Navier for the harmonic load distribution illustrated in figure 9 and defined by:

$$\underline{p}(x, y) = -p_0 \sin\left(\frac{\pi x}{L_1}\right) \sin\left(\frac{\pi y}{L_2}\right) \underline{e}_3 \tag{34}$$

where p_0 is a constant and $L_1 = n_1 L$, $L_2 = n_2 L$, where n_1 and n_2 stand for the numbers of repeated unit-cells in x- and y-direction respectively.

According to standard theory of elastic plates, the moment distribution is given by:

$$M(x, y) = \frac{p_0}{\left(\frac{\pi^2}{L_1^2} + \frac{\pi^2}{L_2^2}\right)} \sin\left(\frac{\pi x}{L_1}\right) \sin\left(\frac{\pi y}{L_2}\right) \tag{35}$$

and the transverse displacement by:

$$u_3(x, y) = \frac{p_0}{D\left(\frac{\pi^2}{L_1^2} + \frac{\pi^2}{L_2^2}\right)^2} \sin\left(\frac{\pi x}{L_1}\right) \sin\left(\frac{\pi y}{L_2}\right) \tag{36}$$

where D is the equivalent bending stiffness established in (29).

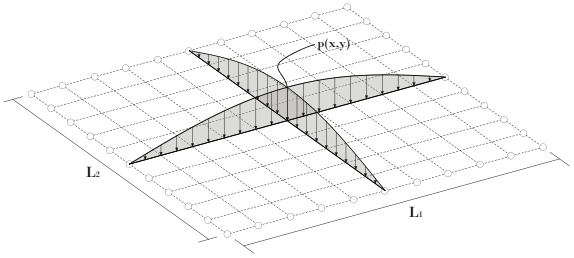

Fig. 9. Nexorade configuration with load applied

5.2. Finite element simulation

The finite element simulations have been conducted with ABAQUS using the linear Timoshenko beam model. An equivalent distributed line load has been calculated from the distribution given by Equation 34. Simple plate supports along the line have been replaced by spherical joints on members ends. Inner connections are all made of spherical joints in conformity with the model hypotheses (with torsion blocked at one end to avoid rigid motion). Every member has been meshed with 10 elements. Every analyse presented here is linear elastic.

From a geometrical point of view, the analytical model established in section 3 has shown that the bending stiffness was independent of the choice of the members directions relatively to those of the plate. Their directions is thus varied along with φ to ease automatic generation by periodicity. With reference to Figure 4, a reciprocal system can be described by:

- n_1 and n_2: the numbers of unit cells in direction 1 and 2,
- L_1 and L_2: the total span of the grid,
- $\frac{L_1}{n_1} = \frac{L_2}{n_2} = L$, or scale ratio, which defines the dimension of the unit-cell, which is the same in both direction,
- φ, the rotation angle spanned by the nexorade with the cartesian axis of the plate.

Practically here, the beams will always have a rectangular cross section of $h = 0.3m$, $b = 0.2m$ and their elastic properties will be defined with $E = 1GPa$ and $\nu = 0.3$. The plate will always be a square with $50m$ edges. Typical results of the simulations are hence illustrated in Figures 10a, 10b and 10c where the configurations shown have a scale ratio of 10 and a rotation angle of $\varphi = \arctan\frac{1}{2}$ (or equivalently $a/l = 3$).

Table 1 and Table 2 show the comparison between the analytical model and the FE simulations for a scale ratio of 10. It can be seen that there is a very good agreement between the stresses and displacements found by analytical means and the numerical ones, and this for every values of φ. Using Navier solution for moments (35) and displacements (36) with the expressions given in (29) for the stiffness and in (23) and (22) for inner stresses in is thus perfectly reliable. The analytical model presented here can thus be applied to any other reciprocal surface relying on any plane surface provided that the hypothesis of scale separation is satisfied.

Table 1: Comparison between analytical solution and FEM: Forces

φ	Shear $[N]$			Moment $[Nm]$		
	An.	Aq.	%	An.	Aq.	%
4°	1820	1832	0.7	637	635	0.3
26.6°	316	325	2.8	723	708	2.1
41°	256	269	5.0	866	839	3.2

Table 2: Comparison between analytical solution and FEM: Displacements

φ	Displacement $[m]$		
	An.	Aq.	%
1°	0.395	0.377	4.6
26.6°	0.0.391	0.388	0.6
41°	0.411	0.411	0.2

Indeed, homogenisation techniques require that the scales of the microstructure and macrostructure are separated. Generally, it is admitted that one order of magnitude should be enough. In the specific case of the elastic reciprocal systems studied here, a convergence study has been conducted. The unit-cell dimension has been varied ($L = [2.5, 5, 10, 25]$) keeping the overall span at $L_1 = L_2 = 50m$. Three values of φ have been considered. Section and material characteristics are kept unchanged. The complete results of this study are shown in Table 3 and illustrated in Figure 11. It can be seen that the relative error between the analytical model and the numerical solution decrease quickly with the number of unit-cell

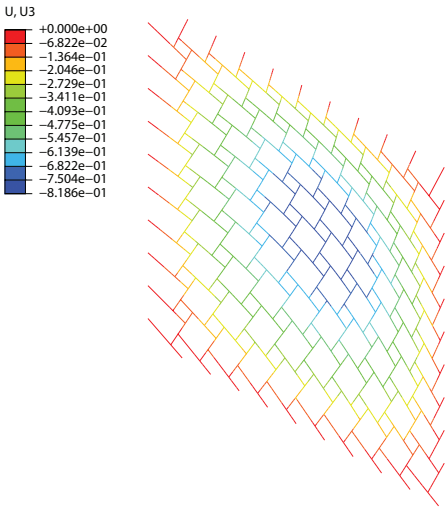

(a) Out-of-plane displacement

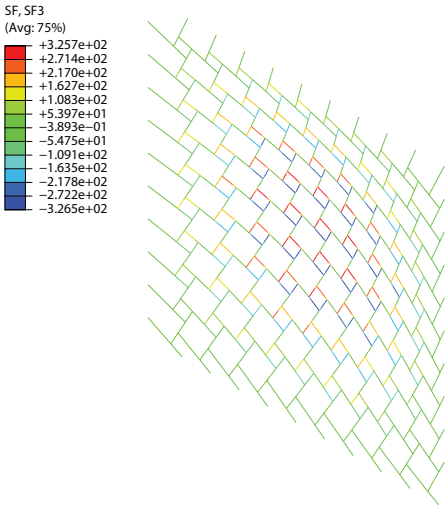

(b) Out-of-plane shear

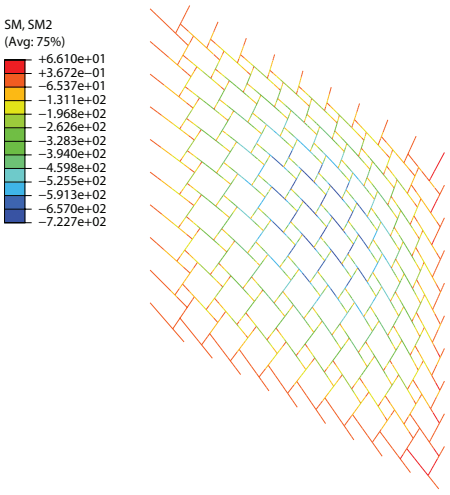

(c) Out-of-plane moment

Fig. 10. FEM results

Table 3: Comparison between analytical model and FEM: Convergence.

L (m)	φ	Displacement $[m]$		Error
		An.	Aq.	%
2.5	1	1.576	1.555	1.3
	$\arctan\frac{1}{2}$	1.446	1.443	0.20
	44.9	1.492	1.492	0.0
5	1	0.3954	0.3770	4.6
	$\arctan\frac{1}{2}$	0.3907	0.3882	0.6
	44.9	0.4108	0.4116	0.2
10	1	0.100	0.0815	18.1
	$\arctan\frac{1}{2}$	0.1136	0.1098	3.3
	44.9	0.1237	0.1249	1.0
25	1	0.0163	0.0126	22.6
	$\arctan\frac{1}{2}$	0.0277	0.0258	7.0
	44.9	0.0330	0.0360	9.0

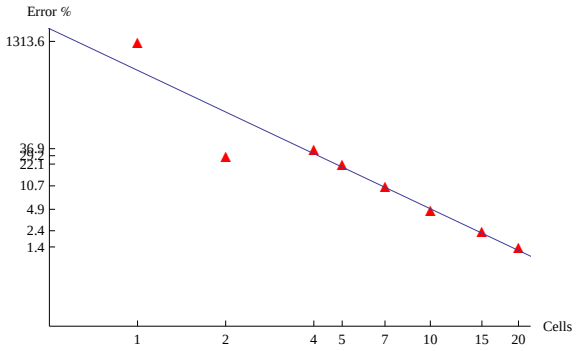

Fig. 11. Convergence study for $\varphi = arctan(1/2)$ ($a/l = 3$): relative error between analytical model and FEM.

with a slope of approximatly 2 meaning that doubling the number of cells divides the error by 4. As expected the error drops bellow 5% for more than 10 unit-cell by edges.

6. CONCLUSION

In this paper, we endeavoured to develop design formulas for reciprocal systems using homogenisation techniques. After recalling basic features of the homogenization theory allowing to consider a beam structures as an equivalent plates, they focused on a specific planar configuration of reciprocal systems made of regular quadrangles. From the closed form solution that they have obtained, they deduced that the studied reciprocal system reduces to a degenerated Kirchhoff-Love plate with following properties:

- no macroscopic torsion bending is achievable inside the structure, the equivalent plate is thus free to deform locally as a hyperbolic paraboloid,
- only strictly bi-axial bending is generating elastic energy,
- the elastic behaviour of plate is thus isotropic, independent of the relative directions of the equivalent plate and of the members.

Then a parametric study of the model revealed that:

- shear forces only depends on the relative engagement length a/l but not on the length l of the members, on the contrary to the bending moment which depends linearly on l, decreasing the size of the members will thus decrease bending stresses but will have no influence on the shear stresses which will remain constant;
- the relative engagement length a/l has a limited influence on the bending stresses which vary from $0.82Ml$ to Ml but there is an optimal configuration which minimises bending stresses for $a/l = (1 - \sqrt{(2)}/2$.
- the relative engagement length a/l has an significant influence on the bending stiffness which is maximum between $a/l = 0.4$ for low value of the members shear stiffness and $a/l = 0.5$ for infinite shear stiffness of the members.

The homogenized approach has been validated numerically using finite element method:

- the displacements and inner forces of the reciprocal systems converge toward the homogeneous plate when the scale ratio (defined as the ratio between the characteristic length of the plate and that of a member) diminishes,
- for a scale ratio of 10 (10 members along the length), the error of the homogeneous model is lower than 5% for all relative engagement length.

In further work, the authors would like to use the same homogenisation techniques to investigate the membrane behaviour of reciprocal systems and by there to provide complementary information on second order effects on the bending behaviour of such systems.

7. REFERENCES

[1] PopovicLarsen, O, *Reciprocal Frame Architecture*, Elsevier (2008).

[2] Baverel, O. and Popovic-Larsen, O., *A Review of Woven Structures with Focus on reciprocal Systems-Nexorades*, International Journal of Space Structures Vol. 26 , No. 4 (2011), pp. 281–288.

[3] Brocato, M. and Mondardini, L., *A new type of stone dome based on Abeilles bond*, International Journal of Solids and Structures Vol. 49 , No. 13 (2012), pp. 1786 –1801.

[4] Douthe, C. and Baverel, O., *Design of nexorades or reciprocal frame systems with the dynamic relaxation method*, Computers & Structures Vol. 87 , No. 21-22 (2009), pp. 1296–1307.

[5] Sanchez, J. and Escrig, F., *Frames Designed by Leonardo with Short Pieces. An analytical Approach*, International Journal of Space Structures Vol. 26 (2011), pp. 289–302.

[6] Baverel, O. et al., *Nexorade*, International Journal of Space Structures Vol. 15 (2000), pp. 155–159.

[7] Gelez, S., Aubry, S., and Vaudeville, B., *Behavior of simple Nexorade or Reciprocal Frame System*, International Journal of Space Structures Vol. 26 (2011), pp. 331–342.

[8] Gelez, S., Aubry, S., and Vaudeville, B., *Nexorade or Reciprocal Frame System Applied to the Design and Construction of a 850 m2 Archaeological Shelter*, International Journal of Space Structures Vol. 26 , No. 4 (Dec. 2011), pp. 303–312.

[9] Sanchez-Palencia, E, *Non-Homogeneous Media and Vibration Theory*, ed. by Sanchez-Palencia, E, vol. 127, Lecture Notes in Physics 127, Berlin, Heidelberg: Springer Berlin Heidelberg (1980), p. 398.

[10] Lebée, A. and Sab, K., *Homogenization of a space frame as a thick plate: Application of the Bending-Gradient theory to a beam lattice*, Computers & Structures (Mar. 2013).

[11] Whitney, J. M. and Leissa, A. W., *Analysis of Heterogeneous Anisotropic Plates*, Journal of Applied Mechanics Vol. 36 , No. 2 (1969), p. 261.

[12] Caillerie, D., *Thin elastic and periodic plates*, Mathematical Methods in the Applied Sciences Vol. 6 , No. 1 (June 1984), pp. 159–191.

[13] Song, P. et al., *Reciprocal Frame Structures Made Easy*, ACM Transactions on Graphics Vol. 32 , No. 4 (2013).

[14] Brocato, M., *Reciprocal frames: Kinematical determinacy and limit analysis*, International Journal of Space Structures Vol. 26 (2011), pp. 343–358.

[15] Baverel, O, Nooshin, H, and Kuroiwa, Y., *Configuration processing of nexorades using genetic algorithms*, Journal of the International Association for Shell and Spatial Structures Vol. 45 , No. 2 (2004), 99108.

[16] Lorato, A et al., *The transverse elastic properties of chiral honeycombs*, Composites Science and Technology Vol. 70 , No. 7 (July 2010), pp. 1057–1063.